Mapping erosion-corrosion of carbon steel in oil-water solutions: effects of velocity and applied potential

M. M. Stack and G. H. Abdulrahman

Department of Mechanical Engineering

University of Strathclyde

75 Montrose Street

G1 1XJ

Glasgow. UK

margaret.stack@strath.ac.uk

Phone No: 44 141 548 3754
Fax No: 44 141 552 5105

Abstract

In this study, the combined effects of erosion and corrosion on carbon steel were investigated in three environments containing crude oil, reservoir water, and a mixture of both solutions at a range of applied potentials, velocities and impact angle. The results indicate that the corrosion contribution was augmented with an increase in the percentage of reservoir water. Both the erosion and corrosion contributions increased with impact velocity for all three environments. Following exposure of the carbon steel in the crude oil, the extent of the erosion was greater than that of corrosion, whilst in the reservoir water, the erosion and corrosion contributions were similar. Mechanisms of erosion-corrosion were proposed based on the change in erosion behaviour at various impact angles and applied potentials in the various environments. Erosion-corrosion maps were constructed based on the results, showing the change in mechanisms and wastage rates as a function of impact velocity and applied potential at various impact angles.

1. Introduction

In oil production, the presence of sand, combined with various salts and gases results in erosion-corrosion of tubing in downstream and upstream oilfields [1--4]. Sand production from oil reservoir conditions can be controlled by design of a gravel pack which prevents it from combining with oil in the process of transportation from downstream to upstream conditions [2]. In such conditions, corrosion occurs due to H_2S and CO_2 [2, 3]. Prediction of the service life of the material in oil production activities under these conditions is approached with some difficulty [3]. Erosion-corrosion is thus a serious issue in oil fields, both in onshore and offshore conditions, because it can cause significant degradation to materials used in the transportation process and has led to development of various test rigs to simulate the process [5].

In the literature on tribo-corrosion, there have been attempts to separate the erosion, corrosion and interaction between the processes using various techniques [6-9]. This is important, as the effects of corrosion on erosion and erosion on corrosion on material degradation can lead to different modes of degradation on the material surface. Quantification of these components of the interaction can facilitate analysis of material loss mechanisms and development of predictive models of material lifetime [10-15].

Progress in the understanding of erosion-corrosion of materials has been achieved by the development of erosion-corrosion diagrams showing mechanisms of damage as a function of the main erosion-corrosion variables [3, 4, 6, 13-15]. Such mechanistic maps provide an important tool for monitoring the mechanistic changes in erosion-corrosion as a function of a multi-parameter set. However, to date such maps have rarely been used for application to oil /water conditions.

In this paper, the effects of impact velocity, impact angle and applied potential were assessed for carbon steel in a range of crude oil/water slurries. Erosion-corrosion maps were generated based on the results showing the variation in wastage and regime of degradation as a function of these variables. The potential applications of such maps to such materials issues in oil/water conditions are addressed in this paper.

2. Experimental details

2.1. Erosion-corrosion test methods

The erosion–corrosion tests were carried out using an impinging jet apparatus, as shown in Fig.1 [5]. The apparatus consisted of a jet of particles in an aqueous flow enabling the effect of erosion variables to be evaluated independently of each other. The impact angle of the specimen could be varied by rotating the stationary specimen. The velocity was calibrated through knowledge of the geometry of the outlet jet. The slurry was composed of Al_2O_3 between 600-710 μm Fig. 2(a-b), in a buffer solution of Na_2CO_3 + $NaHCO_3$. The pH value was 8.3. The test specimen was connected to an electrochemical cell as shown elsewhere (4) and the reference electrode was Saturated Calomel.

Potentiodynamic polarization curves were measured through sweeping the potential in a positive direction from −800 to 800 mV at a sweep rate of 200 mV min^{-1}. Erosion–corrosion tests were conducted at five applied potentials namely, -400 mV,-200 mV, 0 mV, 200 mV and 400mV (SCE) for 30 minutes using a computer controlled ACM potentiostatic to fix the potential at the required value. The test material was carbon steel supplied by Kelvin Steel Glasgow with chemical composition as percentage: C: 0.18, Mn 1.6, Si 0.55, Cr 0.25, Cu: 0.35, Ni: 0.3, S: 0.008. The chemical composition of crude oil in ppm (mass) was (Ca: 33.26, Na: 4.26, K: 1.07, H_2S: 0.0007). The specific gravity was 0.7674 and density was 767 g l^{-1}.

The dimensions of the specimens were 25mm × 10mm × 4 mm. The area exposed to impingement jet was 0.19cm^2, whilst the remaining area was covered by a coating in order to ensure that all corrosion measurements related to the erosion-corrosion process only.

Mass change measurements were made of the samples post testing using a Metter electronic balance. The tests were carried out at two impact angles i.e. 15°, 90° and three velocities i.e. 2.5, 3.5 and 4.5 m s^{-1}, for 30 minutes. The reproducibility of the experiments was estimated to be ± 5% calculated between two consecutive experiments. Following exposure, the samples were cleaned with distilled water to remove any deposited material, and were subsequently evaluated using Scanning Electron Microscopy.

3. Results

3.1 Electrochemical monitoring

Electrochemical polarization was conducted under potentiodynamic conditions to observe the effects of erosion-corrosion on the carbon steel. The effect of erosion-corrosion on carbon steel in water environment at an impact velocity and impact angle 2.5 m s^{-1} and 15°, Fig. 3(a) showed that the corrosion current densities were increased in a positive direction with higher water content in the slurry. In the crude oil environment, it was clear that the free corrosion potential Ecorr had a higher value compared to that in the combined environments and the value of the cathodic current was greater than that of the anodic current. At impact angles of 90°, in the water environment, the anodic current density shifted to higher values with increases in the impact angle from 15° to 90°, Fig. 3(b).

With an increase in the impact velocity to 3.5 m s^{-1} in the crude oil environment, there was an increase in the current densities recorded for all the test conditions, Fig.4 (a), with a similar increase at higher impact angles, Fig. 4(b), Figs. 3-4. At 4.5 m s^{-1}, Fig.5 (a) and 15°, the current density values tended to shift to higher values and thus the values of corrosion contribution were higher at 4.5 m s^{-1} than at 3.5 m s^{-1}. A similar pattern of increase in corrosion current density was observed at higher impact angles, Fig. 5(b), at the higher velocities.

3.2. Volume loss

The weight change during erosion-corrosion can be given as follows;

$$Kec = Ke + Kc \quad (1)$$

$$Ke = Keo + \Delta Ke \quad (2)$$

$$Kc = Kco + \Delta Kc \quad (3)$$

where Kec is total erosion-corrosion rate, Keo is the erosion rate in absence of corrosion, Kco is the corrosion rate in the absence of erosion, ΔKe is the effect of corrosion on the erosion rate and ΔKc is the effect of erosion on the corrosion rate.

The individual contributions are given in Tables 1-6 at the various impact velocities.
The values of Kc were calculated from the Faradaic conversion of the corrosion current density to mass loss. From Figs. 6 (a)-11(a), for carbon steel in the reservoir water, it was clear that the values of the corrosion contribution Kc were lower than those of the erosion contribution Ke in the same environment.

For carbon steel in the crude oil environment, Figs.6 (b)-11(b), the value of the corrosion contribution Kc in the crude oil was less than that in the reservoir water environment and the oil/water environment. The value of Ke was greater in this environment than in the other conditions due to less corrosion occurring under these conditions, Fig. 3-5. In the oil/water conditions, Figs. 6(c)-11(c), the overall value of Kec was lower than that in the water conditions, Fig. 6(a)-11(a), which was also attributed to the lower corrosion rates in such conditions.

Scanning electron microscopy, Figs.12 -13, showed differences in the surfaces for exposure to the various environments. The surface of the specimens in the water environment exhibited a rougher morphology, Fig. 12(a), compared to that in the crude oil environment, Fig. 12(b), and the oil/water water environment, Fig. 12(c). Increases in velocity resulted in a significant increase in plastic deformation, with evidence of greater indentation of metal and corrosion film in such conditions, Fig. 13 (a-c).

4. Discussion

4.1. Effect of applied potential and impact velocity.

For the carbon steel in the reservoir water, the general trend is for the corrosion current densities to increase with increase in impact velocity, Figs.3-5(a). This is possibly due to the effects of repeated impacts removing the film and thus increasing the charge required for re-passivation. For the carbon steel in the crude oil and reservoir water/oil, a similar pattern of an increase in corrosion current density is observed, at 90°, Figs.3-5 (b). However, the extent of such increases is not as high compared to those for carbon steel in the reservoir water, probably due to the higher corrosion resistance of the oil film.

It is interesting that the total erosion–corrosion mass losses Kec, Figs.6-11(b-c) are significantly lower for the carbon steel in crude oil and oil/water compared with the carbon steel in reservoir water. For the carbon steel in reservoir water, there is evidence of an increase in Kc with increases in impact angle from 15° to 90° at all impact velocities consistent with observations from previous work [3-4].

4.2. Erosion-corrosion maps

The erosion-corrosion mechanism maps show transition regimes between erosion-corrosion, corrosion-erosion, and corrosion mechanism as a function of Ke/Kc [4, 6]:

$Ke/Kc < 0.1$	Corrosion-dominated	(4)
$1>Ke/Kc \geq 0.1$	Corrosion-erosion	(5)
$10>Ke/Kc \geq 1$	Erosion-corrosion	(6)
$Ke/Kc \geq 10$	Erosion-dominated	(7)

where Ke and Kc are the erosion and corrosion contributions respectively.

Tables 1 to 6 show the methodology for calculating the values of boundaries (Ke/Kc).
The corrosion process can either be dissolution, passivation, transpassivation, or pitting [3, 4 and 6]. Wear maps have also used in micro-abrasion to characterize the particle motion transitions in abrasive contacts [16].

The erosion–corrosion mechanism maps, Figs.14-15, demonstrate that the boundaries for carbon steel in the crude oil and water/oil environments are unlike to those of the reservoir water environment.

In the reservoir water, at lower impact angles15°, the erosion –dissolution regime is observed at the low lower potential range, Fig.14 (a). At higher potentials, there is the transition from erosion- passivation to passivation-erosion for carbon steel in the reservoir water, as velocity is increased in the low velocity range. This may be attributed to the formation of oxide films on the surface of specimen in the anodic conditions, as increases in velocity are associated with increases in oxygen concentration to the surface [7]. The shift in the regime back to erosion-passivation behaviour, at further increases in velocity, indicates that the corrosion products tend to be removed at higher-impact velocities, in the anodic regime Fig.14 (a).

In the crude oil conditions, the map is dominated by erosion-dominated behaviour, Fig. 14 (b), indicating corrosion is low compared with erosion in such conditions, and consisting with the polarization and mass loss data, Figs, 3-11..

In the crude oil/water conditions, Fig, 14 (c), the transitions between erosion dissolution and erosion passivation shift to higher potentials below 3.5 ms^{-1} and to lower potentials above 3.5 ms^{-1}. This is possibly due to the competing effects of erosion, the increased oxygen concentration to the surface at higher velocities and the shielding presence of the oil film on the surface.

At 90 ° impact angles, in reservoir water, Fig. 15(a), the passivation-erosion regime dominates in anodic conditions, unlike that observed at lower impact angles, Fig. 14(a). This may be due to a change in corrosion mechanism at the higher impact angles. For the crude oil, Fig. 15(b), erosion-dominated behaviour is the main material loss mechanism, similar to that observed at lower impact angles, Fig. 14(b). There is no evidence of any corrosion regime, which is attributed to the role of oil film in reducing the mass loss due to corrosion. For the crude oil/water conditions, Fig. 15(c), the effect of velocity appears to increase the predominance of the erosion-passivation regime, as the potential is swept in a positive direction. At these higher impact angles, the extent of erosion-dissolution is greater than at lower impact angles, Fig. 14(c).

Erosion–corrosion wastage maps can be used to demonstrate the differences between levels of wastage as a function of velocity and electrochemical potential. The low-wastage regime correspond to wastage between less or equal to 6 mg cm $^{-2}$ h^{-1}, the intermediate region between 6 and mg cm $^{-2}$ h^{-1}, and 50 mg cm $^{-2}$ h^{-1} and the high-wastage region, values greater than 50 mg cm $^{-2}$ h^{-1}.[3,4 and 6]. From the results of erosion–corrosion wastage maps Figs.16-17(a-c) it is interesting that the crude oil environments provide the optimum protection against corrosion and erosion at the impact angle, velocities and potentials considered in this study.

The protective nature of the oil film is more evident at lower impact velocities i.e. 2.5 ms^{-1} where the higher resistance of the oil film limits the extent of the medium wastage regime at anodic dissolution potentials, Figs. 16 (a-b), for impact at 15°. The map for the crude oil/water environment, Fig. 16(c), is intermediate between those for the reservoir water and crude oil, Figs. 16(a-b). At 90°, the wastage maps show less evidence of the low regime for the reservoir water conditions, Fig. 17(a), compared to that observed at lower impact angles, Fig. 16 (a), in the cathodic region. There is very little difference in the maps for the crude oil conditions at both impact angles, Fig. 16(b)-7(b). However, in the crude oil/water conditions, at higher impact angles, Fig. 17(c), there is an increase in the medium wastage regime compared to that observed at lower impact angles, Fig. 16(c).

Erosion-corrosion additive-synergism maps show the transition in the material degradation with change in the impact velocity and applied potentials. Tables 1 to 6 show the values of ΔKe/ΔKc ratio for the carbon steel in three different environments.
From the following regimes, erosion-corrosion additive-synergism maps can be constructed [3, 4, 6 and 9]

ΔKe/ΔKc <0.1	Additive	(8)
1>Δ Ke/ΔKc≥0.1	Additive-synergistic	(9)
ΔKe/ΔKc>1	Synergistic	(10)

Additive behaviour defines the situation where the enhancement of corrosion due to erosion ΔKc is greater than the effect of corrosion on the erosion ΔKe (erosion due to corrosion) [3-

4]. In cases where corrosion may enhance the erosion ΔKe, this interaction is defined as synergistic behaviour (ΔKe). On the other hand, where it reduces erosion i.e. where the passive film reduces erosion, then the reverse occurs and the mechanism is defined as antagonistic (-ΔKe) [4, 6]. Both synergistic and antagonistic behaviour are characteristics of erosion-corrosion processes [3, 4, 6].

From the results, at impact angles of 15°, it is clear that in the additive region, is highest in water environment, Fig. 18(a). Antagonistic regimes occupy the area at higher potentials possibly due to the protective effect of corrosion products on the surface of specimen Figs.18 (a), at lower velocities. The greater predominace of antagonistic regimes in the crude oil and oil/ water conditions is attributed to the presence of the oil film protecting the surface from erosion, Fig. 18 (b-c). At higher impact angles, Fig. 19 (a-c), the level of antagonism is reduced in all environments, as the impact angle is increased. The fact that the regimes of antagonism "sit" in various windows of conditions in the oil and oil/water slurries, Figs.19 (b-c), possibly indicates different mechanisms of erosion as a function of the variables assessed above.

Further analysis of the volume loss results, as a function of impact angle, Fig. 20 (a-c), Table 7, indicates that that the peak in the value of Kec shifts to lower impact angles with increases in water content in the slurry mixture but that the value of Kc is significantly higher than Ke at 90^{o} than at 15^{o}. Fig. 21-22, illustrate schematically the change in mechanisms of erosion as a function of impact angle, with the highest erosion occurring at lower impact angles for the environments containing water and the reverse occurring for the crude oil conditions. The higher passive film formation at 90^{o} compared to that 15^{o}, indicates different mechanism of material removal as a function of impact angle for the film formed in the water conditions. Clearly, the erosion-corrosion performance in such environments is a function of many variables, with the oil and hydrated films having many different effects on the dynamics of the particle impact.

5. Conclusions

(i)The erosion-corrosion of carbon steel was evaluated in a range of slurry solutions containing oil and water and at various impact angles and applied potentials.

(ii)The results indicated that the mass losses in the aqueous environment were highest in all cases, with the mechanism of erosion-corrosion changing as a function of impact angle and velocity for the oil/water solutions.

(iii) Erosion-corrosion maps have been constructed showing the mechanistic changes and extent of synergy and antagonism as functions of applied potential, impact angle and oil/water content in the slurry solution.

References

[1] G.A. Zhang, Y.F. Cheng, Electrochemical corrosion of X65 pipe steel in oil/water emulsion, Corrosion Science, 51 (2009) 901–907.

[2] R .Hamzah, D.J Stephenson and J.E. Strutt, Erosion of material used in petroleum production, Wear 186 (187) (1995) 493-496.

[3] M.M. Stack, G. Abdulrahman, Mapping erosion-corrosion of carbon steel in oil exploration conditions: Some new approaches to characterizing mechanisms and Synergies, Tribology International, 43 (7) (2010) 1268-1277.

[4] M.M. Stack, T. M. Abd El Badia, Mapping erosion–corrosion of WC/Co–Cr based composite coatings: particle velocity and applied potential effects, Surface& Coatings Technology 201(3-4) (2006) 1335–1347.

[5] J.B. Zu, I.M. Hutchings and G.T. Burstein, Design of a slurry erosion test rig, Wear 140 (2) (1990) 331–344.

[6] M.M. Stack, B.D Jana, Modelling particulate erosion–corrosion in aqueous slurries: some views on the construction of erosion–corrosion maps for a range of pure metals, Wear 256 (2004) 986-1004.

[7] B.R Tian and Y.F. Cheng, Electrochemical corrosion behaviour of X-65 steel in the simulated oil sand slurry. I. Effects of hydrodynamic condition, Corrosion Science 50 (2008) 773-779

[8] Z. Yue, P. Zhou, J. Shi, in: K.C. Ludema (Ed.), Proceedings of the Conference on Wear of Materials, ASME, New York, (1987) 763–768.

[9] M.M. Stack, S. Zhou, R.C. Newman, Identification of transitions in erosion-corrosion regimes in aqueous environments, Wear I86-187 (1995) 523-532.

[10] K. Sasaki, G.T. Burstein, Erosion–corrosion of stainless steel under impingement by a fluid jet Corrosion Science, 49 (1) (2007) 92-102.

[11] A. Gnanavelu, N. Kapur, A. Neville, J.F. Flores, An integrated methodology for predicting material wear rates due to erosion Wear, 267 (11) (2009) 1935-1944

[12] S.S. Rajahram, T.J. Harvey, R.J.K. Wood Electrochemical investigation of erosion–corrosion using a slurry pot erosion tester Tribology International 44 (3) (2011) 232-240.

[13] A. Neville, C. Wang, Erosion–corrosion mitigation by corrosion inhibitors—An assessment of mechanisms Wear 267 (1-4) (2009) 195-203.

[14] S.S. Rajahram, T.J. Harvey, R.J.K. Wood, Full factorial investigation on the erosion–corrosion resistance of UNS S31603 Tribology International 43 (11) (2010) 2072-2083.

[15] M.M. Stack, S.M. Abdelrahman, B.D. Jana, Some perspectives on modelling the effect of temperature on the erosion–corrosion of Fe in aqueous conditions, Tribology International, 43 (12) (2010) 2279-2297.

[16] K. Adachi and I.M.Hutchings, Wear-mode mapping for the micro-scale abrasion test Wear, 255, (1-6) (2003) 23-29.

Captions for figures

Fig 1: Schematic diagram of erosion-corrosion test rig

Fig 2: Optical microscopy of aluminium oxide particles used in the erosion-corrosion test rig :(a) oil (b) Water.

Fig 3: Polarization curves for carbon steel in three environments, at 2.5 m s^{-1}: (a) 15° (b) 90°

Fig 4: Polarization curves for carbon steel in three environments, at 3.5 m s^{-1}: (a) 15° (b) 90°

Fig 5: Polarization curves for carbon steel in three environments, at 4.5 m s^{-1}: (a) 15° (b) 90°
3.5 m s^{-1} (a) 15° (b) 90°

Fig.6: Total volume loss as a function of applied potential for carbon steel at 15° and 2.5 m s^{-1} in (a) water (b) oil and (c) oil / 20% water

Fig.7: Total volume loss as a function of applied potential for carbon steel at 15° and 3.5 m s^{-1} in (a) water (b) oil and (c) oil / 20% water

Fig.8: Total volume loss as a function of applied potential for carbon steel at 15° and 4.5 m s^{-1} in (a) water (b) oil and (c) oil / 20% water

Fig.9: Total volume loss as a function of applied potential for carbon steel at 90° and 2.5 m s^{-1} in (a) water (b) oil and (c) oil / 20% water

Fig .10: Total volume loss as a function of applied potential for carbon steel at 90° and 3.5 m s^{-1} in (a) water (b) oil and (c) oil / 20% water

Fig .11: Total volume loss as a function of applied potential for carbon steel at 90° and 4.5 m s^{-1} in (a) water (b) oil and (c) oil / 20% water

Fig. 12: Scanning electron micrographs of eroded carbon steel test specimen at 2.5 m s^{-1}, -400mV and 15°: (a) water (b) crude oil and (c) oil / 20% water.

Fig. 13: Scanning electron micrographs of eroded carbon steel test specimen at 4.5 m s^{-1} , 400mV and 90°:(a) water (b) oil and (c) oil / 20% water

Fig. 14: Erosion-corrosion mechanism maps for carbon steel in (a) water (b) crude oil and (c) oil / 20% water at 15°.

Fig. 15: Erosion-corrosion mechanism maps for carbon steel in (a) in water (a) in crude oil (c) 20% of water / crude oil at 90°.

Fig. 16: Erosion-corrosion wastage maps for carbon steel in (a) water environment (b) in crude oil (c) 20% of water / crude oil at 15°.

Fig. 17: Erosion-corrosion wastage maps for carbon steel in (a) water environment (b) in crude oil (c) 20% of water / crude oil at 90°.

Fig. 18: Erosion-corrosion additive-synergism maps for carbon steel in (a) in water (b) crude oil (c) 20% of water / crude oil at impact angle 15°.

Fig. 19: Erosion-corrosion additive-synergism maps for carbon steel in (a) in water (b) in crude oil (c) 20% of water / crude oil at 90°.

Fig. 20: Volume loss as function of impact angle for carbon steel at 200 mV and 2.5 m s^{-1} impact velocity in (a) water(b) crude oil (c) oil/ 20% water

Fig. 21: Schematic diagram showing change in mechanism of erosion-corrosion for carbon steel at impact angle 15° in (a) water (b) crude oil (c) oil/20% water.

Fig. 22: Schematic diagram showing change in mechanism of erosion-corrosion for carbon steel at impact angle 15° in (a) water (b) crude oil (c) oil/20% water.

Captions for Tables

Table 1: Volume loss for carbon steel at various potentials and impact angle 15° at 2.5 m s^{-1} (a) water (b) crude oil (c) oil/20% water.

Table 2: Volume loss for carbon steel at various potentials and impact angle 15° at 3.5 m s^{-1} (a) water (b) crude oil (c) oil/20% water.

Table 3:Volume loss for carbon steel at various potentials and impact angle 15° at 4.5 m s^{-1}(a) water (b) crude oil (c) oil/20% water.

Table 4: Volume loss for carbon steel at various potentials and impact angle of 90° at 2.5 m s^{-1} (a) water (b) crude oil (c) oil/20% water.

Table 5: Volume loss for carbon steel at various potentials and impact angle of 90° at 3.5 m s^{-1} (a) water (b) crude oil (c) oil/20% water.

Table 6: Volume loss for carbon steel at various potentials and impact angle of 90° at 4.5 m s^{-1}(a) water (b) crude oil (c) oil/20% water.

Table 7: Volume loss as function of impact angle for carbon steel at applied potential 200mV and impact velocity 2.5 m s^{-1} in (a) water (b) crude oil (c) oil/20% water.

Tables

Table 1: Volume loss for carbon steel at various potentials and impact angle 15° at 2.5 m s^{-1} (a) water (b) oil and (c) oil / 20% water

(a)

mV	Δke	Δkc	Δke/Δkc	Ke/Kc	Ke	Kc	Kec
-400	8.90E-01	-2.10E-01	-4.2	1.5	2.59	1.72	4.31
-200	7.50E-01	-1.40E-01	-5.4	1.4	2.45	1.78	4.23
0	8.80E-01	-1.60E-01	-5.5	1.42	2.58	1.82	4.4
200	7.30E-01	-5.00E-02	-14.6	1.3	2.43	1.95	4.38
400	7.40E-01	-7.00E-02	-10.6	1.24	2.44	1.97	4.41

(b)

mV	Δke	Δkc	Δke/Δkc	Ke/Kc	Ke	Kc	Kec
-400	4.99E-01	1.10E-02	45.4	117.53	2.479	2.11E-02	2.5
-200	6.04E-01	2.20E-03	274	158.5	2.584	1.63E-02	2.6
0	1.403	-6.00E-04	-2337.5	182.8	3.383	1.85E-02	3.401
200	1.781	5.00E-04	3561	193.8	3.761	1.94E-02	3.78
400	1.779	2.90E-03	613	200	4.289	2.14E-02	4.31

(c)

mV	Δke	Δkc	Δke/Δkc	Ke/Kc	Ke	Kc	Kec
-400	3.30E-01	-1.20E-01	-2.8	2.9	2.31	0.8	3.11
-200	3.58E-01	-4.00E-02	-9	2.87	2.338	0.812	3.15
0	8.00E-02	-8.00E-02	-1	2.6	2.06	0.78	2.84
200	1.20E-01	-3.00E-02	-4	3.08	2.1	0.68	2.78
400	-9.00E-02	-9.00E-02	1	2.6	1.89	0.71	2.6

Table 2: Volume loss for carbon steel at various potentials and impact angle 15° at 3.5 m s^{-1} (a) water (b) oil and (c) oil / 20% water

(a)

mV	Δke	Δkc	Δke/Δkc	Ke/Kc	Ke	Kc	Kec
-400	-6.00E-01	1.1	-0.55	1.5	1.4	4.12	5.52
-200	-2.30E-01	7.30E-01	-0.31	0.42	1.77	4.21	5.98
0	-3.50E-01	8.60E-01	-0.40	0.38	1.65	4.38	6.03
200	-2.70E-01	8.70E-01	-0.31	0.39	1.73	4.48	6.21
400	1.49E+00	5.10E-01	2.92	0.77	3.49	4.51	8

(b)

mV	Δke	Δkc	Δke/Δkc	Ke/Kc	Ke	Kc	Kec
-400	2.26	-2.60E-03	-869	241	4.561	1.89E-02	4.58
-200	2.8	-2.20E-03	-1272	244	5.099	2.09E-02	5.12
0	2.77	5.80E-03	478	196	5.074	2.59E-02	5.1
200	3.27	2.00E-03	1637	214	5.574	2.61E-02	5.6
400	4.67	5.00E-04	9348	270	6.974	2.58E-02	7

(c)

mV	Δke	Δkc	Δke/Δkc	Ke/Kc	Ke	Kc	Kec
-400	1.86	-7.00E-02	-26.6	4.95	4.16	0.84	5
-200	2.72	1.10E-01	24.7	5.12	5.02	0.98	6
0	2.81	-3.00E-02	-94	5.74	5.11	0.89	6
200	3.17	1.30E-01	24.4	5.9	5.47	0.93	6.4
400	3.71	2.00E-01	18.6	5.01	6.01	1.2	7.21

Table 3:Volume loss for carbon steel at various potentials and impact angle 15° at 4.5 m s^{-1}(a) water (b) oil and (c) oil / 20% water

(a)

mV	Δke	Δkc	Δke/Δkc	Ke/Kc	Ke	Kc	Kec
-400	-1.00E-02	1.22 E+00	-8.20E-03	5.23E-01	2.99	5.72	8.71
-200	-6.10E-01	1.23 E+00	-4.95E-01	4.09E-01	2.39	5.84	8.23
0	8.20E-01	1.1 E+00	7.45E-01	6.46E-01	3.82	5.91	9.73
200	1.76E+00	2.60E-01	6.8 E+00	9.08E-01	4.76	5.24	10
400	2.25E+00	1.20E-01	18.8 E+00	1.01E+00	5.25	5.2	10.45

(b)

mV	Δke	Δkc	Δke/Δkc	Ke/Kc	Ke	Kc	Kec
-400	3.88	1.00E-03	3871	259	7.471	2.88E-02	7.5
-200	3.64	5.00E-03	728	192	7.242	3.78E-02	7.28
0	4.36	1.80E-03	2421	186	7.957	4.28E-02	8
200	4.83	7.00E-03	689	187	8.425	4.50E-02	8.47
400	4.47	-2.00E-04	-22361	168.9	8.072	4.78E-02	8.12

(c)

mV	Δke	Δkc	Δke/Δkc	Ke/Kc	Ke	Kc	Kec
-400	2.9	-5.00E-02	-57	4.78	6.45	1.35	7.8
-200	3.1	2.00E-01	15.5	5.15	6.7	1.3	8
0	3.7	2.00E-01	18.4	4.85	7.28	1.5	8.78
200	3.74	-2.00E-02	-187	4.4	7.34	1.68	9.02
400	4.01	-1.00E-01	-40.1	4.01	7.61	1.9	9.51

Table 4: Volume loss for carbon steel at various potentials and impact angle 90° at 2.5 m s^{-1}
(a) water (b) oil and (c) oil / 20% water

(a)

mV	Δke	Δkc	Δke/Δkc	Ke/Kc	Ke	Kc	Kec
-400	9.00E-01	-2.00E-01	-4.50E-01	1.42 E+01	2.5	1.71	4.21
-200	3.00E-01	2.80E-01	1.07E+01	8.60E-01	1.9	2.21	4.1
0	-3.00E-01	4.80E-01	-6.25E-02	5.70E-01	1.57	2.73	4.3
200	-3.80E-01	5.00E-01	-7.60E-01	4.40E-01	1.22	2.78	4
400	-1.20E-01	1.00E-01	-1.20E-01	5.90E-01	1.48	2.53	4

(b)

mV	Δke	Δkc	Δke/Δkc	Ke/Kc	Ke	Kc	Kec
-400	4.00E-01	-1.70E-04	-231	116	2.092	1.81E-02	2.11
-200	1.43	7.00E-04	2043	159	3.13	1.97E-02	3.15
0	1.68	5.00E-04	3360	169	3.38	2.00E-02	3.4
200	2.27	5.20E-03	438	164	3.976	2.42E-02	4
400	2.27	7.00E-03	325	150	4.084	2.65E-02	4.11

(c)

mV	Δke	Δkc	Δke/Δkc	Ke/Kc	Ke	Kc	Kec
-400	4.80E-01	2.30E-01	2.01	2.42	2.18	0.9	3.08
-200	1.70E-01	3.00E-01	5.60E-01	2.05	1.87	0.91	2.78
0	4.30E-01	-2.00E-02	-21.5	2.73	2.13	0.78	2.91
200	5.70E-01	-6.00E-02	-9.5	3.11	2.27	0.73	3
400	7.00E-01	2.00E-02	35	3	2.4	0.8	3.2

Table 5: Volume loss for carbon steel at various potentials and impact angle 90° at 3.5 m s^{-1}
(a) water (b) oil and (c) oil / 20% water

(a)

mV	Δke	Δkc	Δke/Δkc	Ke/Kc	Ke	Kc	Kec
-400	-3.00E-01	2.10E-01	-1.43	4.40E-01	1.9	4.31	6.21
-200	-2.30E-01	4.80E-01	-0.48	4.50E-01	1.97	4.38	6.35
0	2.80E-01	9.90E-01	2.80E-01	4.90E-01	2.48	5	7.48
200	3.00E-01	1.61	1.90E-01	4.50E-01	2.5	5.52	8.02
400	-9.00E-02	1.49	-6.40E-02	3.60E-01	2.11	5.81	7.92

(b)

mV	Δke	Δkc	Δke/Δkc	Ke/Kc	Ke	Kc	Kec
-400	2.70	4.70E-03	575	181	4.754	2.62E-02	4.78
-200	2.92	4.90E-03	596	181	4.973	2.74E-02	5
0	3.31	6.90E-03	454	178	5.181	2.91E-02	5.21
200	3.7	7.10E-03	521	191	5.75	3.01E-02	5.78
400	4.42	7.80E-03	566	201	6.468	3.21E-02	6.5

(c)

mV	Δke	Δkc	Δke/Δkc	Ke/Kc	Ke	Kc	Kec
-400	2.95	3.20E-01	9.21	4.54	5	1.1	6.1
-200	3.15	2.00E-02	158	5.2	5.2	1	6.2
0	3.27	2.00E-01	16.35	5.43	5.32	0.98	6.3
200	3.13	4.30E-01	7.28	4.21	5.18	1.23	6.41
400	3.75	3.60E-01	10.4	4.83	5.8	1.2	7

Table 6: Volume loss for carbon steel at various potentials and impact angle 90° at 4.5 m s^{-1}(a) water (b) oil and (c) oil / 20% water

(a)

mV	Δke	Δkc	Δke/Δkc	Ke/Kc	Ke	Kc	Kec
-400	1.79	-7.00E-02	-25.57	9.80E-01	4.69	4.78	9.47
-200	2.58	-5.40E-01	-4.78	1.35	5.48	4.83	10.31
0	0.57	8.30E-01	6.90E-01	5.80E-01	3.47	6.03	9.5
200	1.29	6.3	2.05	6.80E-01	4.19	6.13	10.32
400	1.39	1.03	1.35	6.40E-01	4.29	6.73	11.02

(b)

mV	Δke	Δkc	Δke/Δkc	Ke/Kc	Ke	Kc	Kec
-400	3.94	6.90E-03	571	173	7.139	4.12E-02	7.18
-200	4.56	7.40E-03	616	195	7.76	3.99E-02	7.8
0	4.20	1.04E-02	404	162	7.404	4.56E-02	7.45
200	4.75	9.10E-03	522	166	7.952	4.78E-02	8
400	4.98	1.00E-02	493	158	8.178	5.18E-02	8.23

(c)

mV	Δke	Δkc	Δke/Δkc	Ke/Kc	Ke	Kc	Kec
-400	3.55	2.50E-01	14.2	4.66	6.75	1.45	8.2
-200	3.9	2.90E-01	13.4	4.73	7.1	1.5	8.6
0	3.92	3.00E-01	13	4.5	7.12	1.6	8.72
200	4.7	3.00E-01	16	4.65	7.9	1.7	9.6
400	4.78	-1.10E-01	-43.45	4.22	7.98	1.89	9.87

Table 7: Volume loss as function of impact angle for carbon steel at applied potential 200mV and impact velocity 2.5 m s^{-1} in (a) water (b) crude oil (c) oil/20% water.

(a)

Impact angle	Ke(mg cm^{-2} h^{-1})	Kc(mg cm^{-2} h^{-1})	Kec(mg cm^{-2} h^{-1})
15°	2.43	1.95	4.38
30°	2.56	1.94	4.5
45°	2.58	2.03	4.6
60°	1.5	2.71	4.2
75°	2.26	1.34	3.6
90°	1.22	2.78	4

(b)

Impact angle	Ke(mg cm^{-2} h^{-1})	Kc(mg cm^{-2} h^{-1})	Kec(mg cm^{-2} h^{-1})
15°	3.761	1.94E-02	3.78
30°	3.485	1.49E-02	3.5
45°	3.545	1.51E-02	3.56
60°	3.1	2.00E-02	3.12
75°	3.577	2.33E-02	3.6
90°	3.976	2.42E-02	4

(c)

Impact angle	Ke(mg cm^{-2} h^{-1})	Kc(mg cm^{-2} h^{-1})	Kec(mg cm^{-2} h^{-1})
15°	2.1	0.68	2.78
30°	2.35	0.9	3.25
45°	2.89	0.81	3.7
60°	2.64	0.96	3.6
75°	2.42	0.45	2.87
90°	2.27	0.73	3

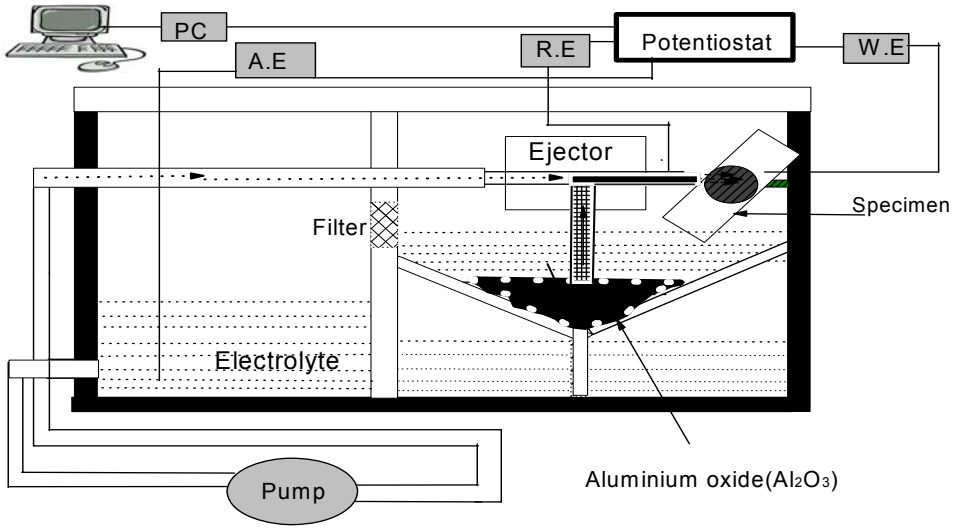

Fig (1): Schematic diagram of erosion-corrosion test rig

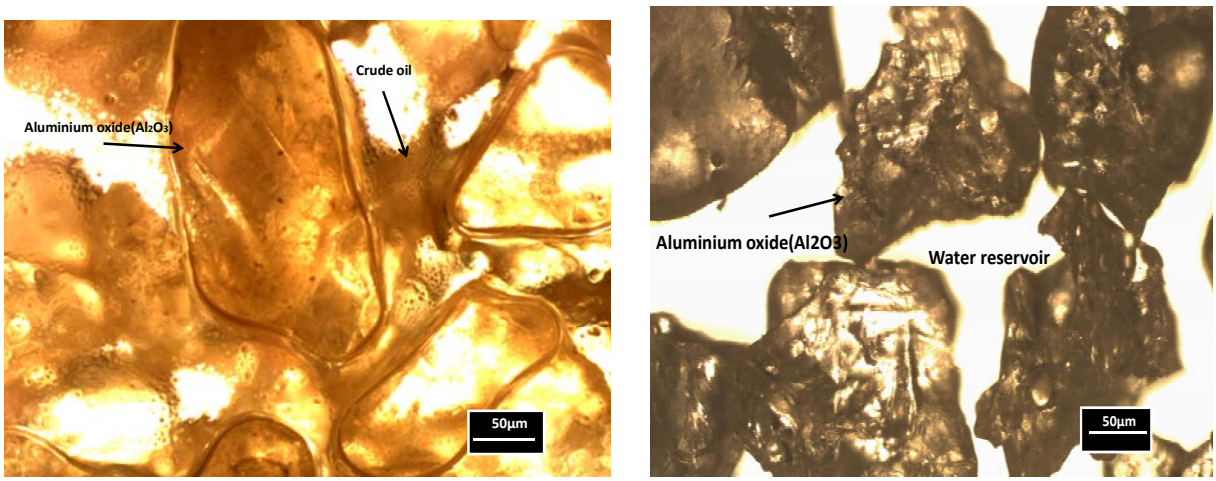

(a) (b)

Fig (2): Optical microscopy of aluminium oxide particles used in the erosion-corrosion test rig: (a) oil (b) Water.

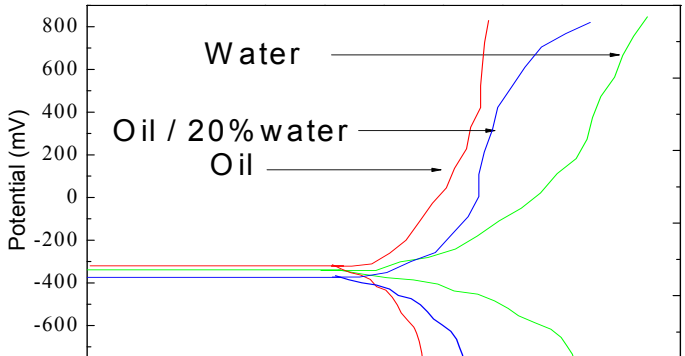

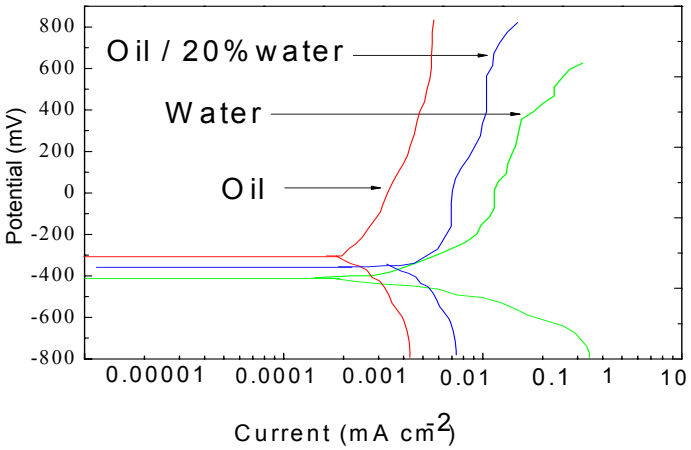

(a) (b)

Fig (3): Polarization curves for carbon steel in three environments, at 2.5 m s^{-1}:(a) 15° (b) 90°

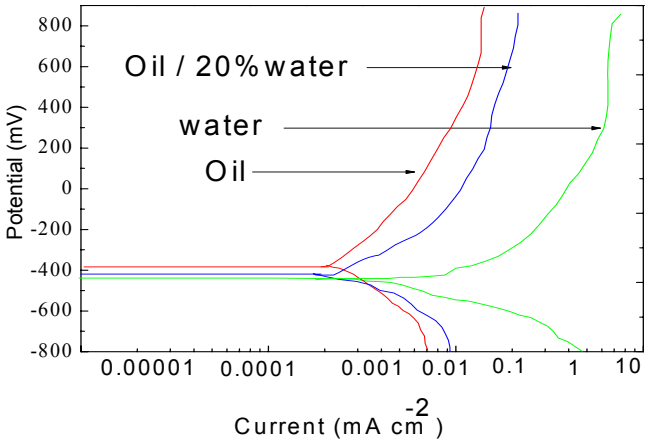

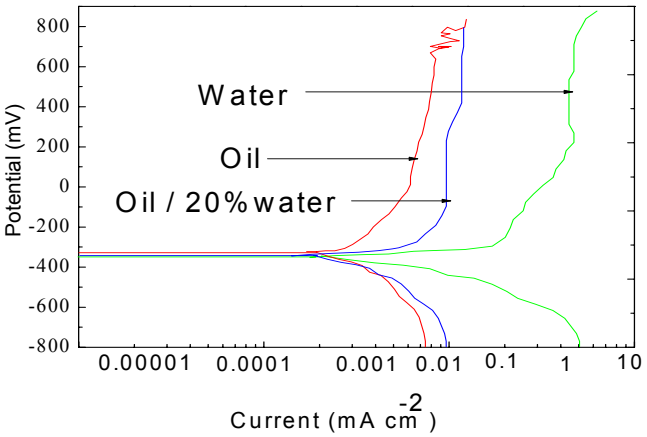

(a) (b)

Fig (4): Polarization curves for carbon steel in three environments, at 3.5 m s^{-1}: (a) 15° (b) 90°

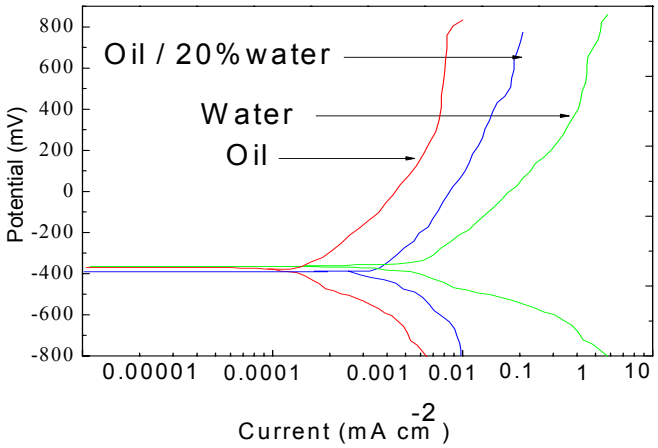

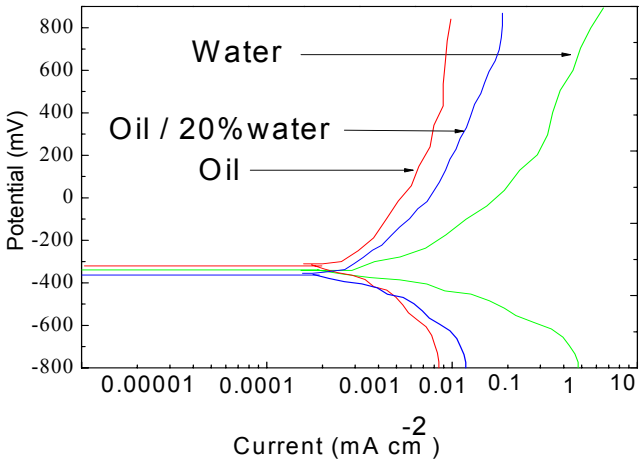

(a) (b)

Fig (5): Polarization curves for carbon steel in three environments, at 4.5 m s^{-1}:(a) 15° (b) 90°

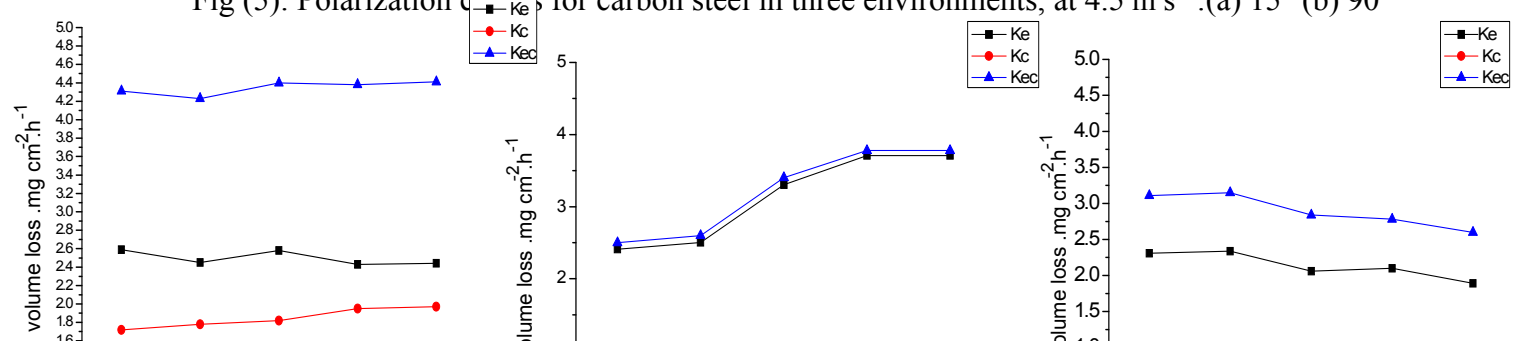

(a) (b) (c)

Fig.(6): Total volume loss as a function of applied potential for carbon steel at impact angle 15° and 2.5 m s^{-1} in (a) water (b) oil and (c) oil / 20% water

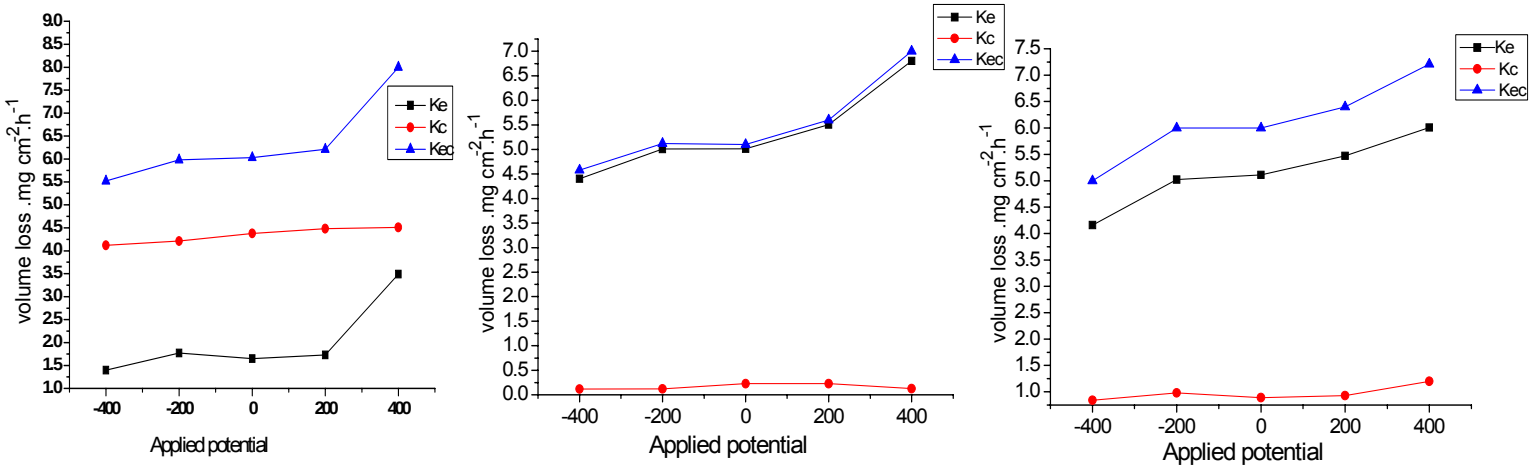

(a) (b) (c)

Fig.(7): Total volume loss as a function of applied potential for carbon steel at impact angle 15° and 3.5 m s^{-1} in (a) water (b) oil and (c) oil / 20% water

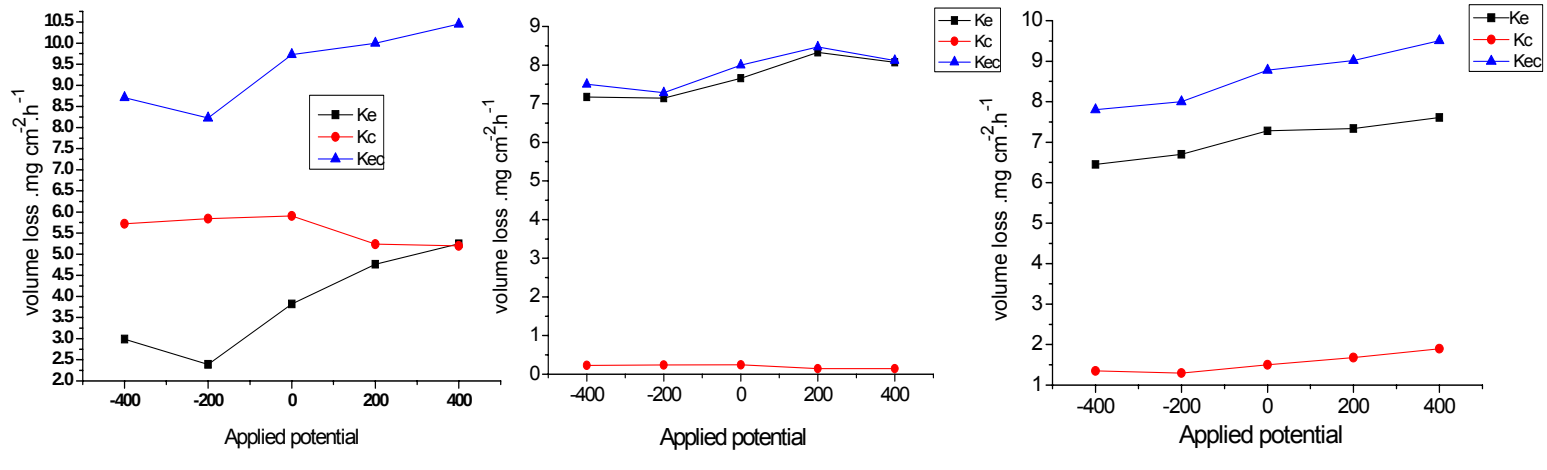

(a) (b) (c)

Fig.(8): Total volume loss as a function of applied potential for carbon steel at impact angle 15° and 4.5 m s^{-1} in (a) water (b) oil and (c) oil / 20% water

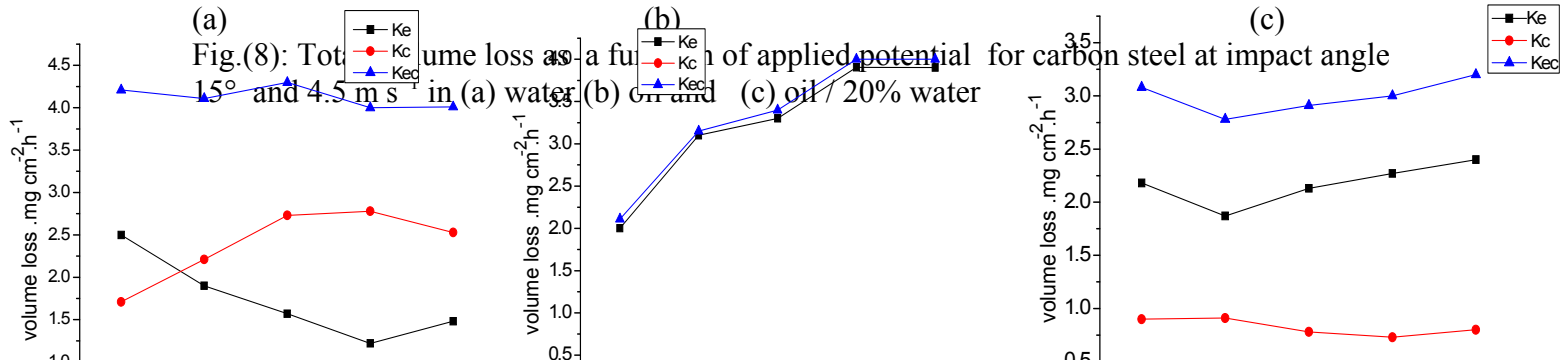

(a) (b) (c)

Fig.(9): Total volume loss as a function of applied potential for carbon steel at impact angle 90° and 2.5 m s^{-1} in (a) water (b) oil and (c) oil / 20% water

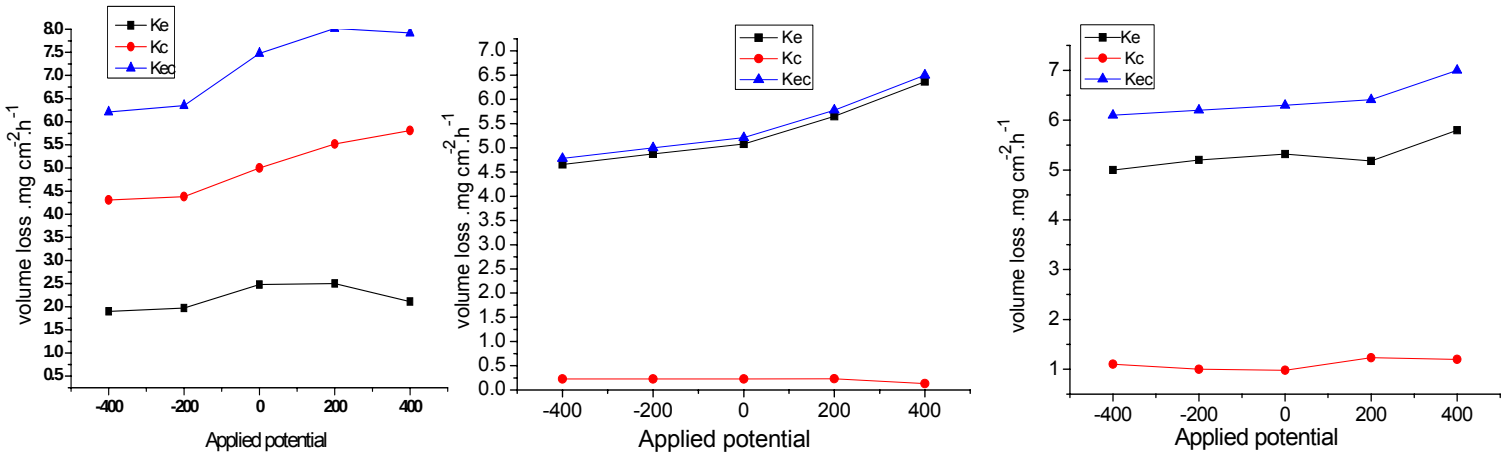

(a) (b) (c)

Fig (10): Total volume loss as a function of applied potential for carbon steel at impact angle 90° and 3.5 m s^{-1} in (a) water (b) oil and (c) oil / 20% water

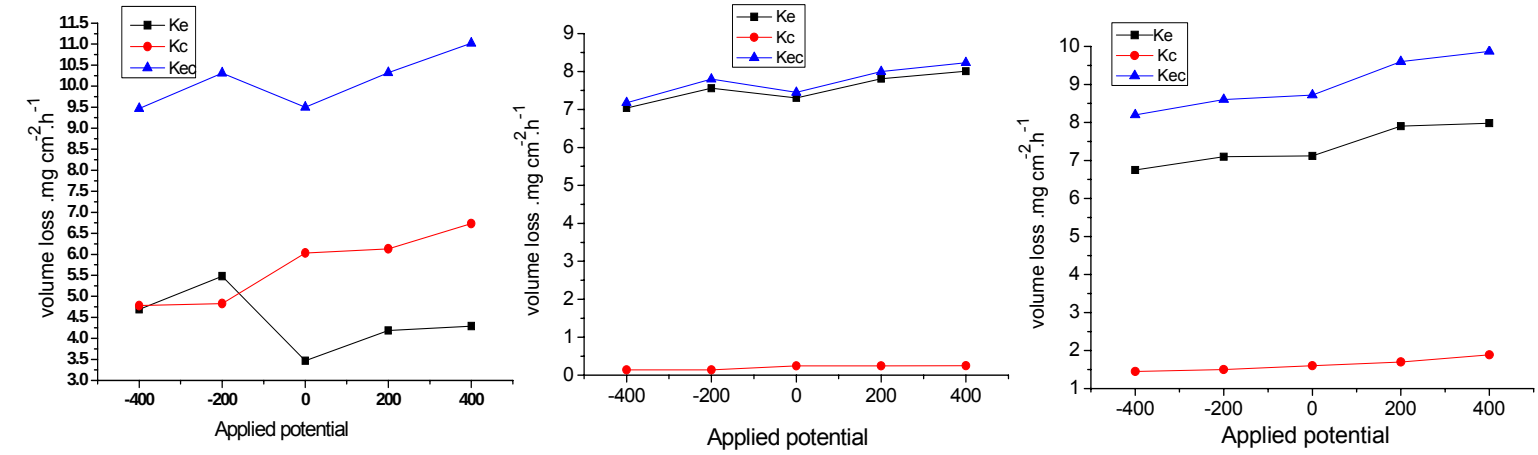

(a) (b) (c)

Fig (11): Total volume loss as a function of applied potential for carbon steel at impact angle 90° and 4.5 m s^{-1} in (a) water (b) oil and (c) oil / 20% water

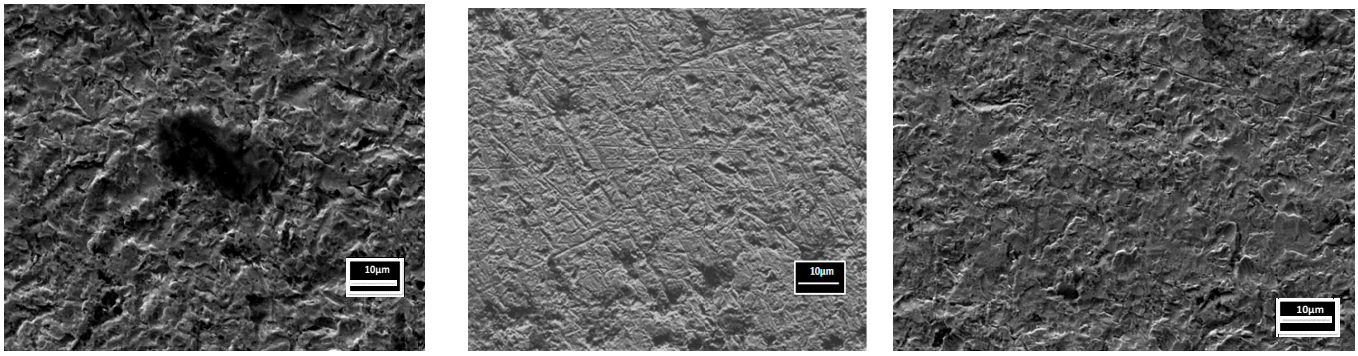

(a) (b) (c)

Fig (12): Scanning electron micrographs of eroded carbon steel test specimen at 2.5 m s^{-1}, -400mV and impact angle 15°: (a) water (b) crude oil and (c) oil / 20% water.

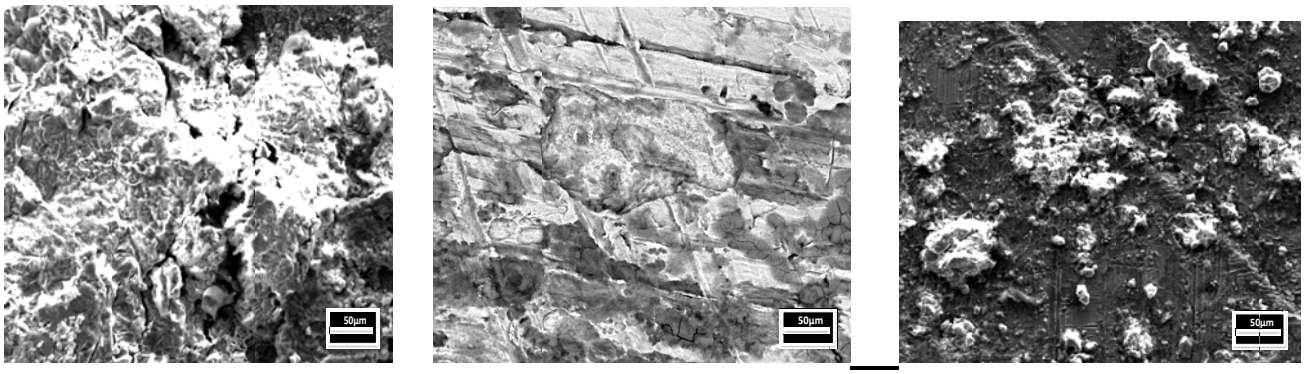

(a) (b) (c)

Fig (13): Scanning electron micrographs of eroded carbon steel test specimen at 4.5 m s^{-1} , 400mV and impact angle 90°:(a) water (b) oil and (c) oil / 20% water.

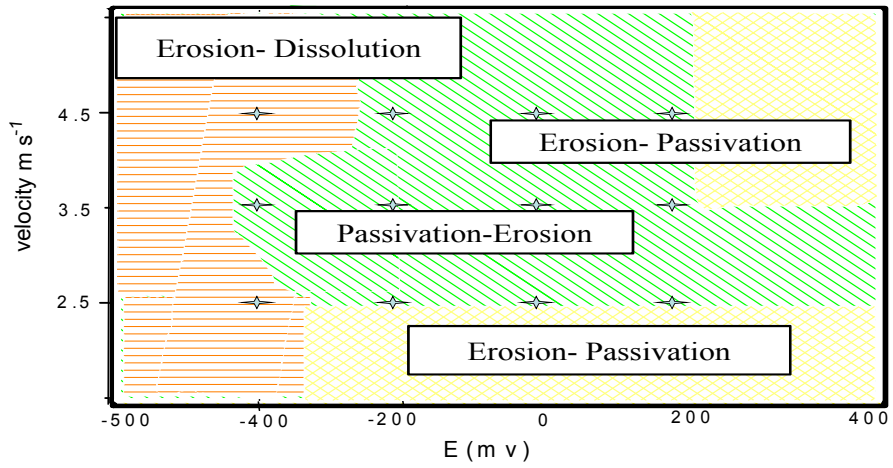

(a)

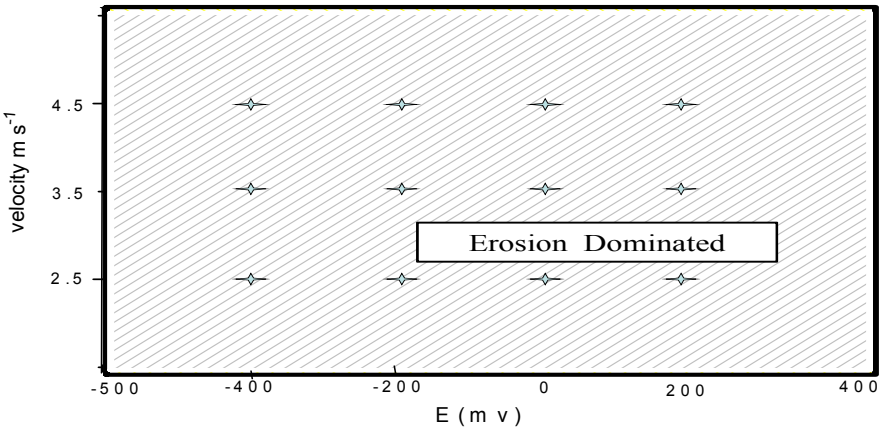

(b)

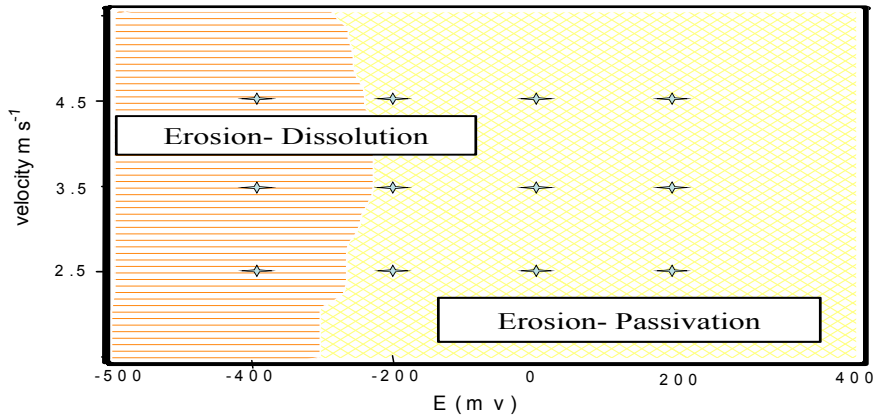

(c)

Fig (14): Erosion-corrosion mechanism maps for carbon steel in (a) water (b) crude oil and (c) oil / 20% water at impact angle 15°.

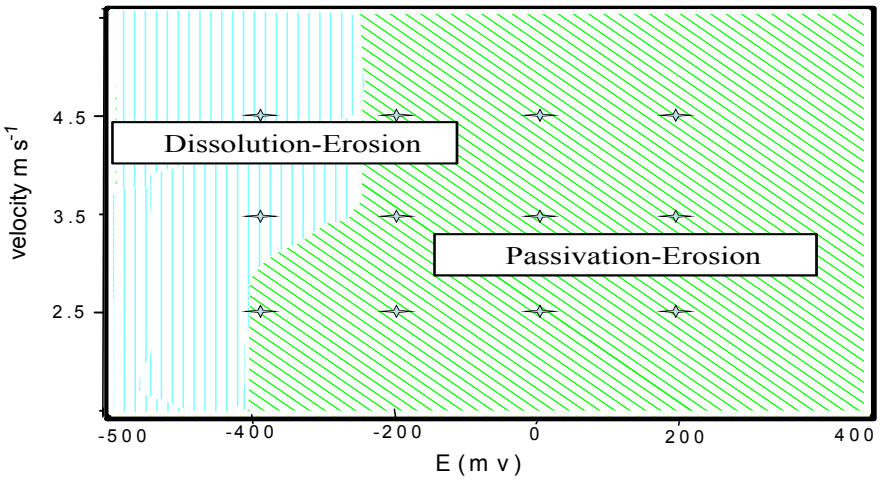

(a)

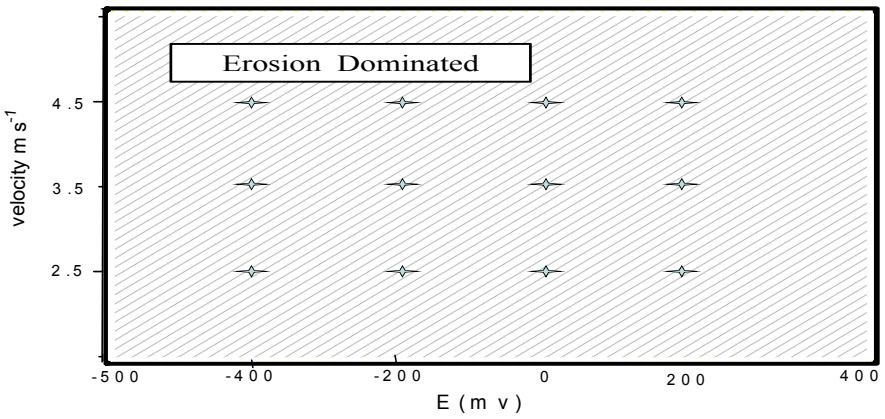

(b)

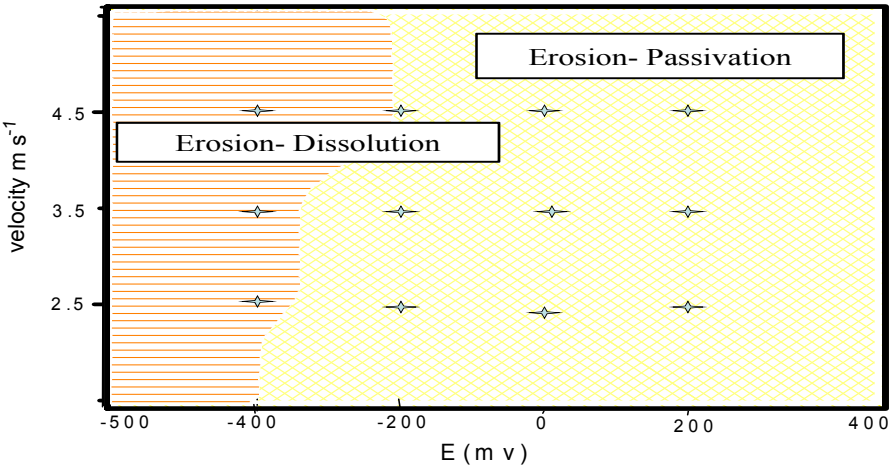

(c)

Fig (15): Erosion-corrosion mechanism maps for carbon steel in (a) in water (b) oil and (c) oil / 20% water at impact angle 90°.

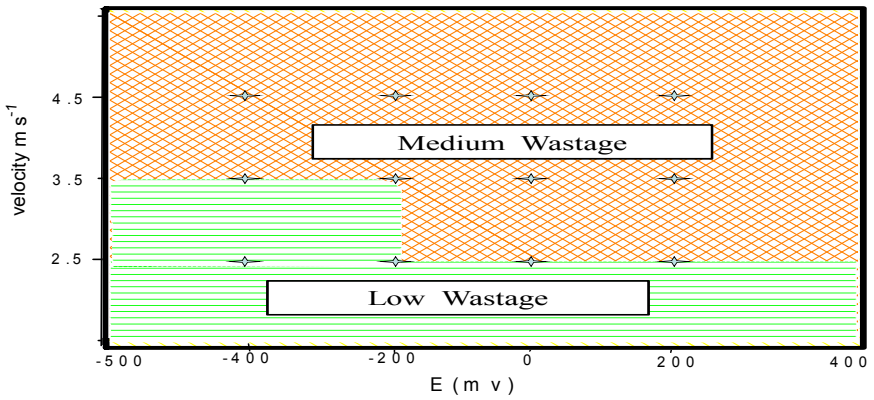

(a)

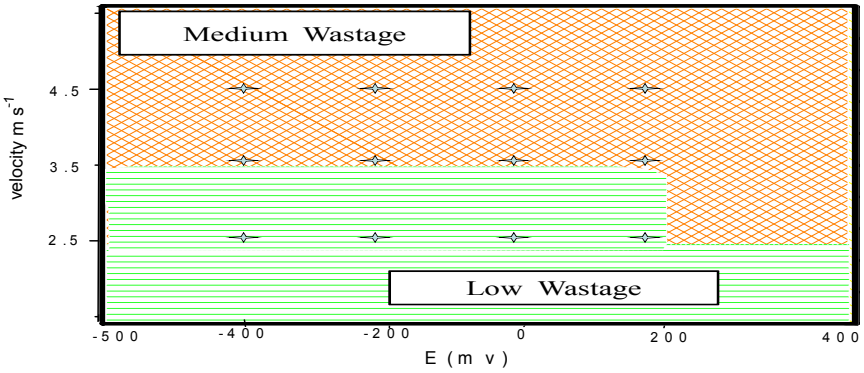

(b)

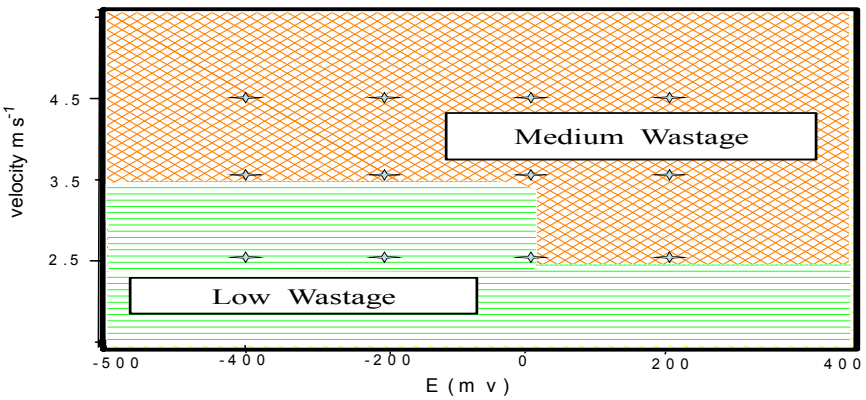

(c)

Fig (16): Erosion-corrosion wastage maps for carbon steel in (a) water (b) oil and (c) oil / 20% water at impact angle 15°.

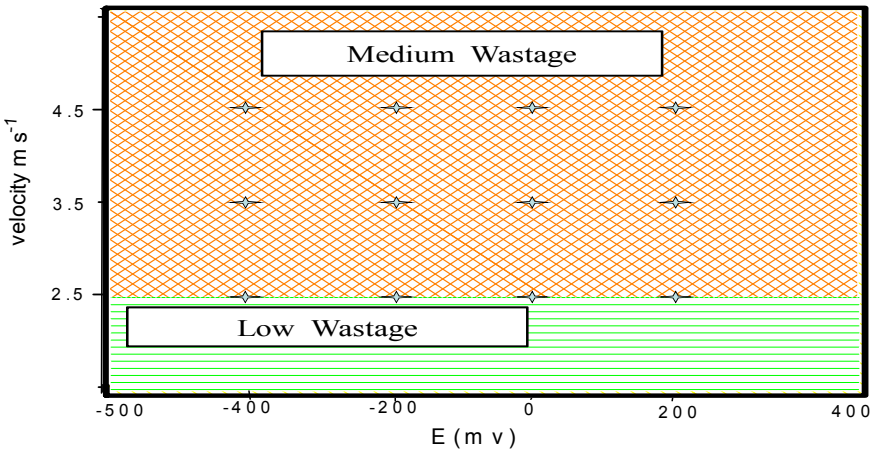

(a)

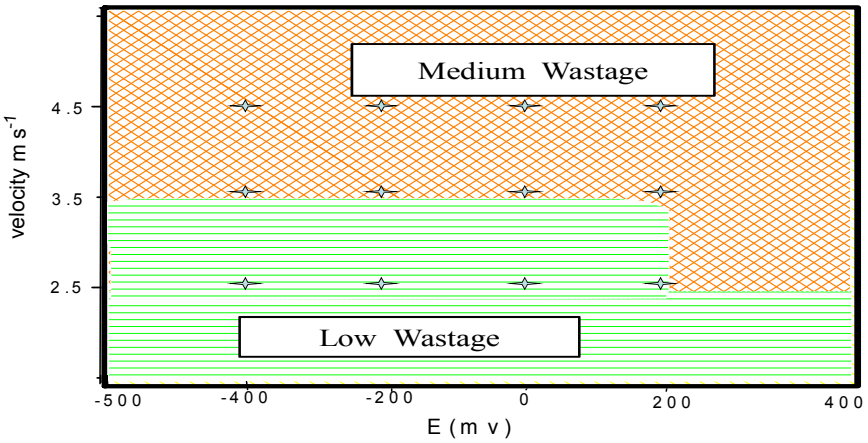

(b)

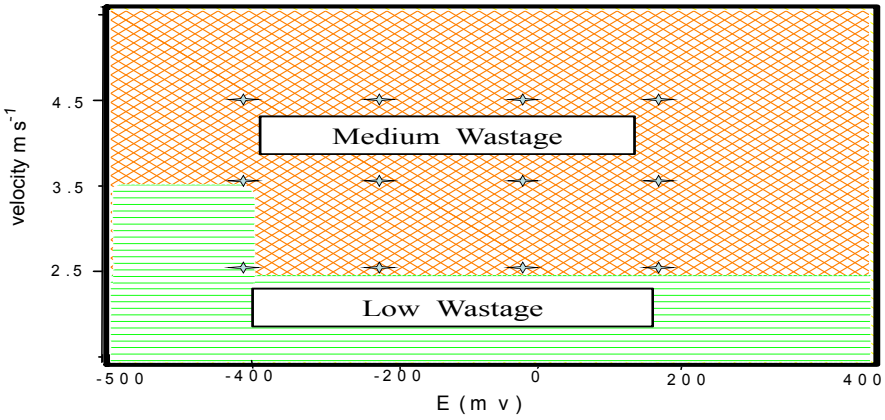

(c)

Fig (17): Erosion-corrosion wastage maps for carbon steel in (a) water (b) oil and (c) oil / 20% water at impact angle 90°.

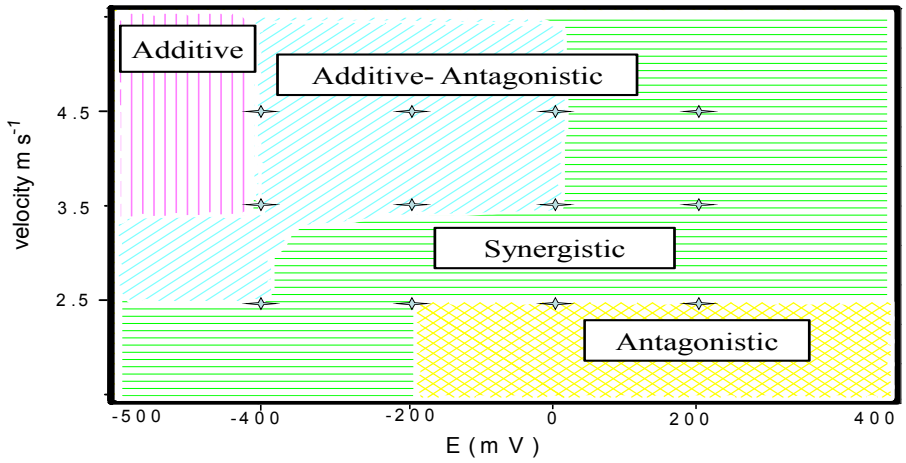

(a)

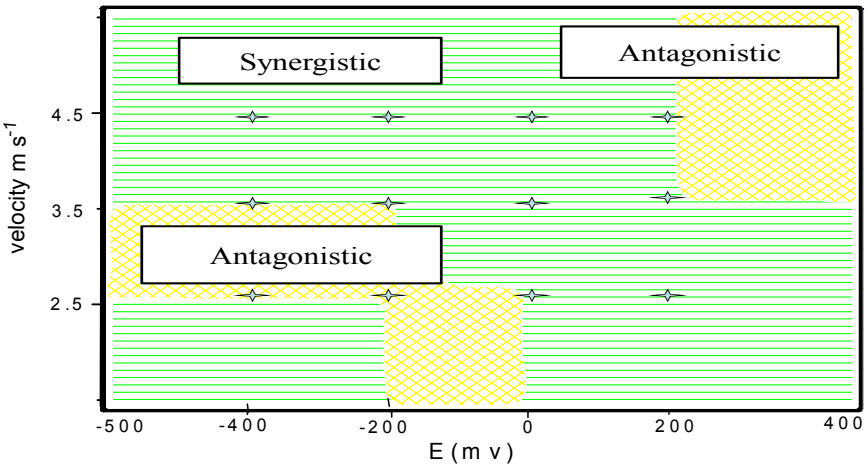

(b)

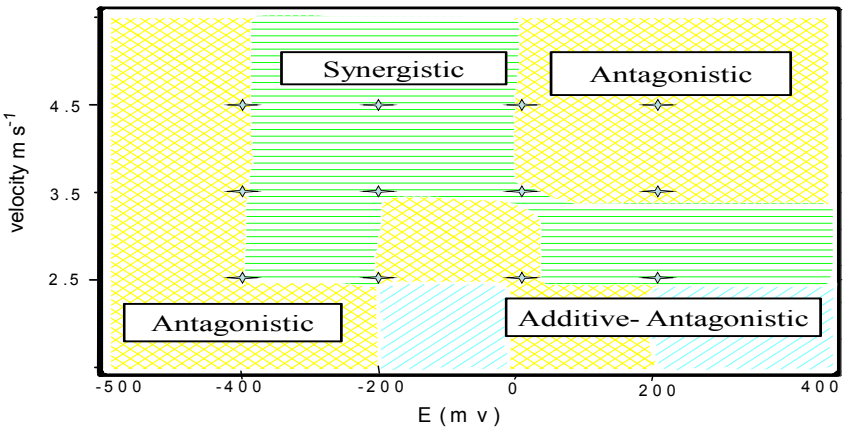

(c)

Fig (18): Erosion-corrosion additive-synergism maps for carbon steel in (a) water (b) oil and (c) oil / 20% water at impact angle 15°

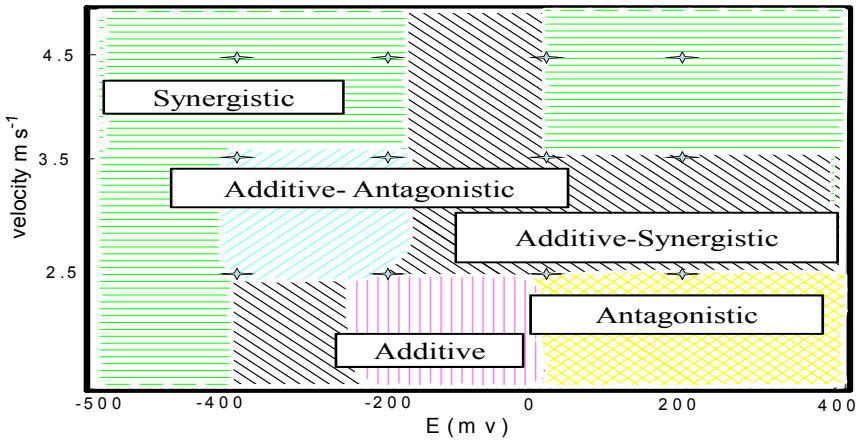

(a)

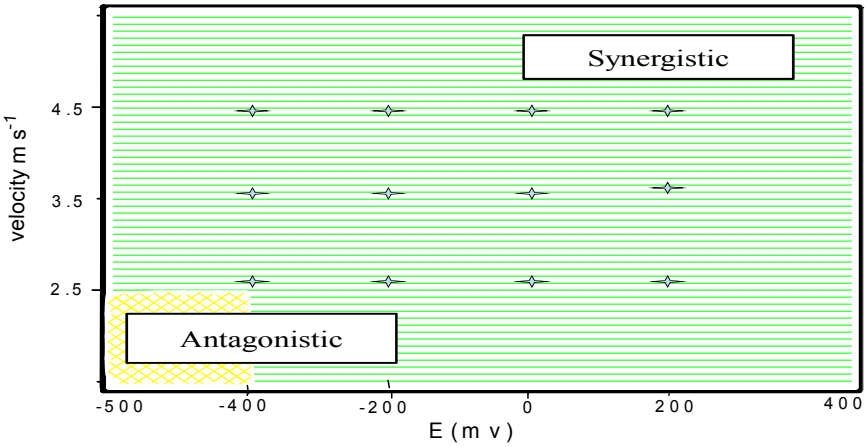

(b)

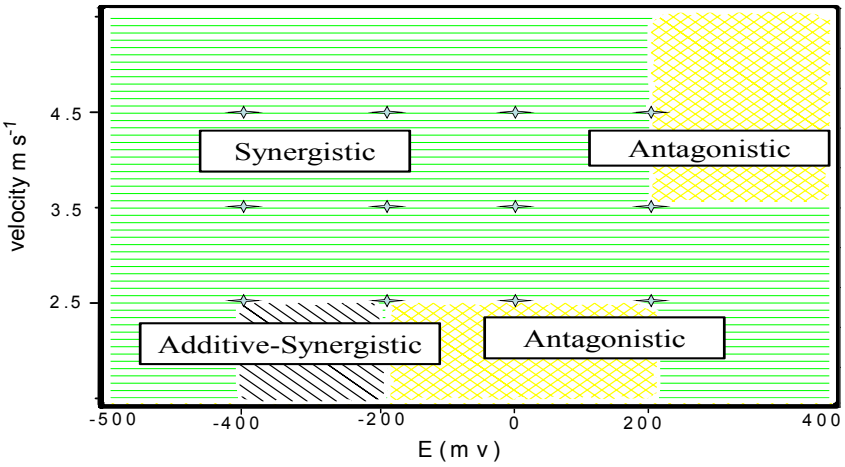

(c)

Fig (19): Erosion-corrosion additive-synergism maps for carbon steel in (a) water (b) oil and (c) oil / 20% water at impact angle 90°.

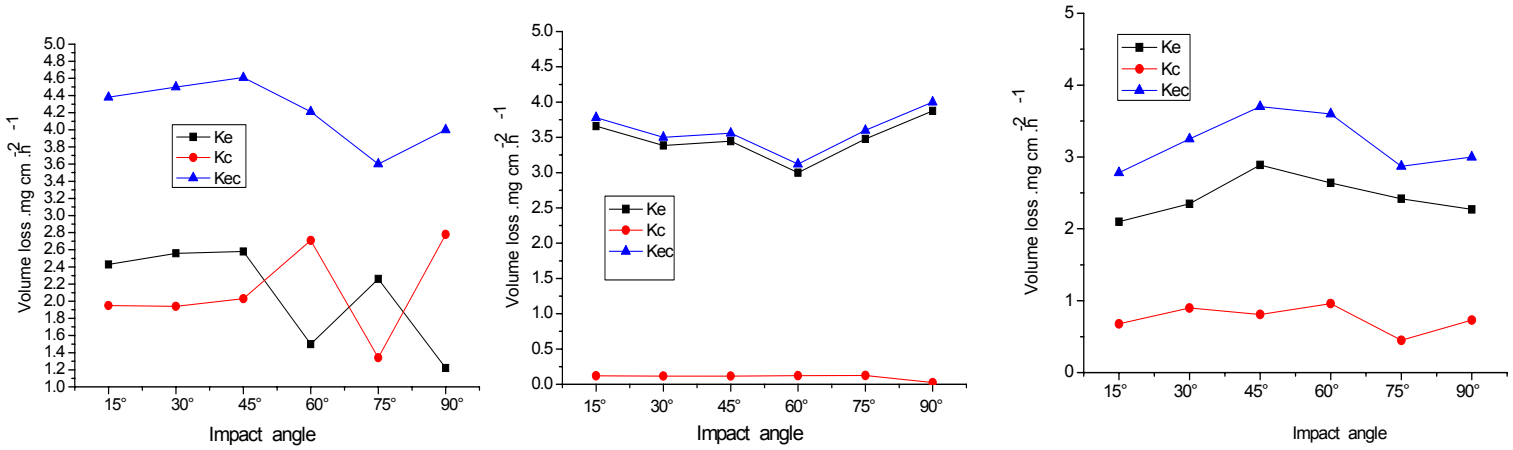

(a) (b) (c)

Fig.20: Volume loss as function of impact angle for carbon steel at 200 mV and 2.5 m s^{-1} impact velocity in (a) water(b) crude oil (c) oil/ 20% water

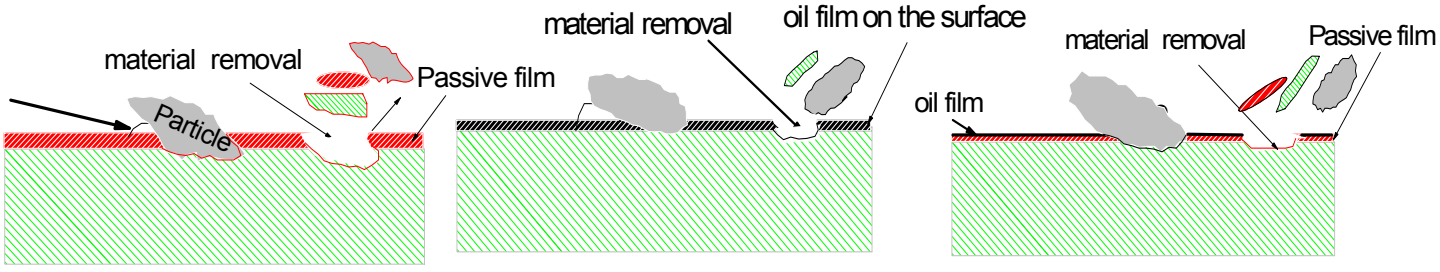

(a) (b) (c)

Fig. 21: Schematic diagram showing changes in mechanism of erosion-corrosion for carbon steel at impact angle 15° in (a) water (b) crude oil (c) oil/20% water.

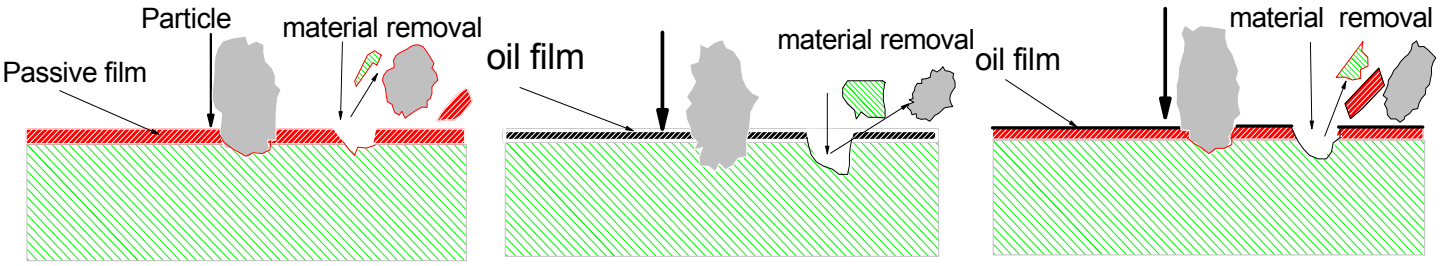

(a) (b) (c)

Fig. 22: Schematic diagram showing changes in mechanism of erosion-corrosion for carbon steel at impact angle 90° in (a) water (b) crude oil (c) oil/20% water.